Thin Films of Bicontinuous Cubic Mesostructured Silica Templated by a Nonionic Surfactant

Ryan C. Hayward,[†] Peter C. A. Alberius,[‡] Edward J. Kramer,[†,§] and Bradley F. Chmelka*,[†]

Department of Chemical Engineering and Materials Department, University of California, Santa Barbara, California 93106, and Institute for Surface Chemistry, Stockholm, Sweden

Received December 30, 2003. In Final Form: March 22, 2004

Thin films of bicontinuous cubic mesostructured silica were formed using the nonionic poly(oxyethylene)-alkyl ether surfactant Brij-56 as a structure-directing agent. The synthesis conditions were chosen such that the estimated volume fraction of surfactant in the silica/surfactant films corresponded approximately to the composition at which the bicontinuous cubic phase occurs in the water/surfactant phase diagram. Small-angle X-ray scattering and transmission electron microscopy measurements reveal that the cubic phase corresponds to the $Ia\bar{3}d$ double-gyroid structure, with some distortion due to anisotropic film shrinkage. The cubic structure grows as faceted domains that are well-oriented with respect to the substrate and often occur in coexistence with a lamellar phase. By adjusting the temperature at which the films are aged, it is possible to create films with 2D hexagonal, cubic, or lamellar structures at a single composition.

Introduction

Thin films of surfactant- and block-copolymer-templated mesoporous silica have attracted considerable recent attention due to the potential applications of these materials as membranes,[1] proton conductors,[2] optical devices,[3] sensors,[4−7] hosts for quantum dots,[8] biocompatible coatings,[9] and low-*k* dielectric insulators,[10−14] to name a few. For many such applications, it is desirable to have a continuous network of uniform mesopores that percolates from one interface to the other. This arrangement would be ideal for applications where selective mass transport of material through the membrane is required, such as for separation processes or to allow access to an active component immobilized in the mesopores.

Several groups have investigated the formation of silica films with templated mesostructures that are analogous to the "micellar" mesophases found in lyotropic systems. These include cubic (I_1) structures[15−21] (space groups $Pm\bar{3}n$ and $Im\bar{3}m$) and 3D hexagonal structures[15−17,21−24] (space group $P6_3/mmc$). Detailed studies, in particular by the group of Terasaki,[25,26] have revealed that the "micellar" mesopores in these structures are often interconnected. There also exists a variety of experimental evidence indicating a degree of pore interconnectivity in such structures that is sufficient to allow transport of small atomic or molecular species such as nitrogen gas,[15] metal ions,[8] and protons[2] between mesopores. For applications involving diffusion of species with sizes that are comparable to the mesopore dimensions, the extent of pore interconnectivity in these materials may not be adequate. The sizes of openings between micellar mesopores have been found in several cases to be substantially smaller than the overall pore size,[25,26] suggesting that the interconnections may present restrictions to mass transport.

One approach to obtaining a 3D interpenetrating system of uniform mesopores without constrictions is to use an

[†] Department of Chemical Engineering, University of California.
[‡] Institute for Surface Chemistry.
[§] Materials Department, University of California.

(1) Tsai, C. Y.; Tam, S. Y.; Lu, Y. F.; Brinker, C. J. *J. Membr. Sci.* **2000**, *169*, 255−268.
(2) Li, H. B.; Nogami, M. *Adv. Mater.* **2002**, *14*, 912−914.
(3) Scott, B. J.; Wirnsberger, G.; Stucky, G. D. *Chem. Mater.* **2001**, *13*, 3140−3150.
(4) Wirnsberger, G.; Scott, B. J.; Stucky, G. D. *Chem. Commun.* **2001**, 119−120.
(5) Arbiol, J.; Cabot, A.; Morante, J. R.; Chen, F. L.; Liu, M. L. *Appl. Phys. Lett.* **2002**, *81*, 3449−3451.
(6) Lu, Y. F.; Han, L.; Brinker, C. J.; Niemczyk, T. M.; Lopez, G. P. *Sens. Actuators, B* **1996**, *36*, 517−521.
(7) Yamada, T.; Zhou, H. S.; Uchida, H.; Tomita, M.; Ueno, Y.; Honma, I.; Asai, K.; Katsube, T. *Microporous Mesoporous Mater.* **2002**, *54*, 269−276.
(8) Besson, S.; Gacoin, T.; Ricolleau, C.; Jacquiod, C.; Boilot, J. P. *Nano Lett.* **2002**, *2*, 409−414.
(9) Gomez-Vega, J. M.; Iyoshi, M.; Kim, K. Y.; Hozumi, A.; Sugimura, H.; Takai, O. *Thin Solid Films* **2001**, *398*, 615−620.
(10) Baskaran, S.; Liu, J.; Domansky, K.; Kohler, N.; Li, X. H.; Coyle, C.; Fryxell, G. E.; Thevuthasan, S.; Williford, R. E. *Adv. Mater.* **2000**, *12*, 291−294.
(11) Yang, S.; Mirau, P. A.; Pai, C. S.; Nalamasu, O.; Reichmanis, E.; Pai, J. C.; Obeng, Y. S.; Seputro, J.; Lin, E. K.; Lee, H. J.; Sun, J. N.; Gidley, D. W. *Chem. Mater.* **2002**, *14*, 369−374.
(12) Yang, S.; Mirau, P. A.; Pai, C. S.; Nalamasu, O.; Reichmanis, E.; Lin, E. K.; Lee, H. J.; Gidley, D. W.; Sun, J. N. *Chem. Mater.* **2001**, *13*, 2762−2764.
(13) Fan, H. Y.; Bentley, H. R.; Kathan, K. R.; Clem, P.; Lu, Y. F.; Brinker, C. J. *J. Non-Cryst. Solids* **2001**, *285*, 79−83.
(14) Wirnsberger, G.; Yang, P.; Scott, B. J.; Chmelka, B. F.; Stucky, G. D. *Spectrochim. Acta, Part A* **2001**, *57*, 2049−2060.
(15) Lu, Y. F.; Ganguli, R.; Drewien, C. A.; Anderson, M. T.; Brinker, C. J.; Gong, W. L.; Guo, Y. X.; Soyez, H.; Dunn, B.; Huang, M. H.; Zink, J. I. *Nature* **1997**, *389*, 364−368.
(16) Zhao, D. Y.; Yang, P. D.; Margolese, D. I.; Chmelka, B. F.; Stucky, G. D. *Chem. Commun.* **1998**, 2499−2500.
(17) Zhao, D.; Yang, P.; Melosh, N.; Feng, J.; Chmelka, B. F.; Stucky, G. D. *Adv. Mater.* **1998**, *10*, 1380−1385.
(18) Ruggles, J. L.; Holt, S. A.; Reynolds, P. A.; Brown, A. S.; Creagh, D. C.; White, J. W. *Phys. Chem. Chem. Phys.* **1999**, *1*, 323−328.
(19) Ogawa, M.; Masukawa, N. *Microporous Mesoporous Mater.* **2000**, *38*, 35−41.
(20) Grosso, D.; Babonneau, F.; Albouy, P. A.; Amenitsch, H.; Balkenende, A. R.; Brunet-Bruneau, A.; Rivory, J. *Chem. Mater.* **2002**, *14*, 931−939.
(21) El-Safty, S. A.; Evans, J. *J. Mater. Chem.* **2002**, *12*, 117−123.
(22) Tolbert, S. H.; Schaffer, T. E.; Feng, J. L.; Hansma, P. K.; Stucky, G. D. *Chem. Mater.* **1997**, *9*, 1962−1967.
(23) Besson, S.; Ricolleau, C.; Gacoin, T.; Jacquiod, C.; Boilot, J. P. *J. Phys. Chem. B* **2000**, *104*, 12095−12097.
(24) Grosso, D.; Balkenende, A. R.; Albouy, P. A.; Lavergne, M.; Mazerolles, L.; Babonneau, F. *J. Mater. Chem.* **2000**, *10*, 2085−2089.
(25) Sakamoto, Y.; Diaz, I.; Terasaki, O.; Zhao, D. Y.; Perez-Pariente, J.; Kim, J. M.; Stucky, G. D. *J. Phys. Chem. B* **2002**, *106*, 3118−3123.
(26) Sakamoto, Y. H.; Kaneda, M.; Terasaki, O.; Zhao, D. Y.; Kim, J. M.; Stucky, G.; Shim, H. J.; Ryoo, R. *Nature* **2000**, *408*, 449−453.

10.1021/la030442z CCC: $27.50
Published on Web 06/11/2004

amphiphilic structure-directing agent that self-assembles into a bicontinuous cubic phase. Such phases consist of co-continuous polar and nonpolar domains, as first shown by Luzzati and Spegt.[27] Bicontinuous cubic structures where the nonpolar species are in the minority (denoted V_1) are comprised of uniformly sized hydrophobic rods that branch in a regular fashion to yield 3D ordered networks.[28,29] The use of such phases to direct the structure of a cross-linking sol (e.g., silica) followed by subsequent removal of the organic templating species results in a mesoporous structure with percolating networks of uniformly sized pore channels. The best-known example of such a material, MCM-48,[30,31] was formed using a quaternary alkylammonium surfactant as a template. The structure of MCM-48 (space group $Ia\bar{3}d$) was found to consist of two enantiomorphic 3D pore networks that are related to Schoen's minimal gyroid surface.[32−35] This structure is analogous to that of the $Ia\bar{3}d$ phase found in lipid- and surfactant-based lyotropic liquid crystals[28] and block-copolymer melts.[36] The name "double-gyroid" has been suggested to denote the presence of two independent, nonintersecting networks of the minority component.[37]

In addition to MCM-48, a number of other bicontinuous silica mesostructures have been templated using a variety of organic species.[21,38−45] While there have been reports of the production of MCM-48 as thick films[46] and embedded in a macroporous membrane,[47] the large majority of work on bicontinuous silica mesostructures has been conducted on powders or monolithic samples. To date, only Thomas and co-workers[41] have investigated the preparation of continuous thin films of such materials, and their approach relies on the use of a specialty silicon-containing block copolymer template synthesized by anionic polymerization.

Recently, we have described an approach for the predictive control of mesostructural ordering in thin films of poly(ethylene oxide)−poly(propylene oxide)−poly(ethylene oxide) triblock-copolymer-templated silica by quantitative comparison to the binary block copolymer/water phase diagram.[48] Here this general approach is put to stringent test, namely, the synthesis of films with technologically important bicontinuous cubic silica mesostructures, which are typically accessible only over narrow ranges of composition. In the current study, we employ a recently published temperature−composition ($T-x$) phase diagram for mixtures of water and the nonionic surfactant Brij-56,[49] which contains a V_1 cubic-phase region over a small composition window, as a guide for the formation of continuous thin films of mesostructured silica. X-ray scattering and transmission electron microscopy results show that this approach offers a straightforward and predictive route for the preparation of mesoporous silica films with a V_1 bicontinuous cubic phase, specifically the $Ia\bar{3}d$ double-gyroid structure.

Experimental Section

The binary phase diagram for mixtures of water with the nonionic poly(oxyethylene) alkyl ether surfactant Brij-56[49] was used as a quantitative guide for preparing mesostructured silica films from multicomponent solutions under nonequilibrium conditions, according to an approach described previously[48] and outlined briefly here. The volume fraction of surfactant in the mesostructured Brij-56/silica films was estimated by taking the volume of the silica sol−gel component to be equal to that of the dense silica formed by complete framework cross-linking, plus the volume of water released by the condensation of $Si(OH)_4$. The volume fraction of surfactant in the film was matched to the desired point on the surfactant/water phase diagram, and this composition was used as a starting point for film syntheses. The synthesis conditions were subsequently adjusted to produce the desired bicontinuous cubic structure (∼5% adjustment in the estimated volume fraction was necessary). In the binary phase diagram for Brij-56/water,[49] the bicontinuous cubic phase occurs within the range of ∼60−70 vol % surfactant and only at temperatures above ∼30° C. Thus, to obtain the desired V_1 phase, films were transferred to a heat stage after dip-coating and subsequently maintained at a given temperature (±1 °C) for at least 15 min. This length of time was adequate to allow silica cross-linking to proceed sufficiently to preserve the mesophase structure.

To prepare bicontinuous cubic mesostructured surfactant/silica films, 1.12−1.16 g of Brij-56 (corresponding to an estimated surfactant content of 59−60 vol % in the dip-coated films) was dissolved in 2.0 g of ethanol, yielding a slightly cloudy solution. Separately, 2.60 g of tetraethyl orthosilicate, 3.0 g of ethanol, and 1.35 g of aqueous hydrochloric acid ([HCl] = 0.032 N, pH 1.5) were mixed and stirred at room temperature for 20 min. All chemicals were obtained from Aldrich and used as received. Subsequently, the two solutions were combined, and films were prepared by dip-coating on aluminized Kapton substrates (Sheldahl) at a speed of ∼0.5 mm/s. All films were prepared within the first 1.5 h of mixing the solutions; storage of the solutions for significantly longer intervals reduced the reliability of the cubic mesostructure being obtained. The organic components were removed by calcining the films in air with a heating rate of 1 °C/min to a temperature of 300 °C, which was maintained for at least 5 h.

To verify the composition of Brij-56 (nominally reported as $C_{16}EO_{10}$), matrix-assisted laser desorption/ionization time-of-

(27) Luzzati, V.; Spegt, P. A. *Nature* **1967**, *215*, 701−704.
(28) Charvolin, J.; Sadoc, J. F. *J. Phys.* **1987**, *48*, 1559−1569.
(29) Luzzati, V.; Vargas, R.; Mariani, P.; Gulik, A.; Delacroix, H. *J. Mol. Biol.* **1993**, *229*, 540−551.
(30) Beck, J. S.; Vartuli, J. C.; Roth, W. J.; Leonowicz, M. E.; Kresge, C. T.; Schmitt, K. D.; Chu, C. T. W.; Olson, D. H.; Sheppard, E. W.; McCullen, S. B.; Higgins, J. B.; Schlenker, J. L. *J. Am. Chem. Soc.* **1992**, *114*, 10834−10843.
(31) Kresge, C. T.; Leonowicz, M. E.; Roth, W. J.; Vartuli, J. C.; Beck, J. S. *Nature* **1992**, *359*, 710−712.
(32) Schoen, A. H. *NASA Technical Note D-5541*; National Aeronautics and Space Administration: Washington, DC, 1970.
(33) Monnier, A.; Schüth, F.; Huo, Q.; Kumar, D.; Margolese, D.; Maxwell, R. S.; Stucky, G. D.; Krishnamurty, M.; Petroff, P.; Firouzi, A.; Janicke, M.; Chmelka, B. F. *Science* **1993**, *261*, 1299−1303.
(34) Alfredsson, V.; Anderson, M. W. *Chem. Mater.* **1996**, *8*, 1141−1146.
(35) Carlsson, A.; Kaneda, M.; Sakamoto, Y.; Terasaki, O.; Ryoo, R.; Joo, S. H. *J. Electron Microsc.* **1999**, *48*, 795−798.
(36) Hajduk, D. A.; Harper, P. E.; Gruner, S. M.; Honeker, C. C.; Kim, G.; Thomas, E. L.; Fetters, L. J. *Macromolecules* **1994**, *27*, 4063−4075.
(37) Avgeropoulos, A.; Dair, B. J.; Hadjichristidis, N.; Thomas, E. L. *Macromolecules* **1997**, *30*, 5634−5642.
(38) Attard, G. S.; Glyde, J. C.; Göltner, C. G. *Nature* **1995**, *378*, 366−368.
(39) Attard, G. S.; Edgar, M.; Göltner, C. G. *Acta Mater.* **1998**, *46*, 751−758.
(40) McGrath, K. M.; Dabbs, D. M.; Yao, N.; Aksay, I. A.; Gruner, S. M. *Science* **1997**, *277*, 552−556.
(41) Chan, V. Z. H.; Hoffman, J.; Lee, V. Y.; Iatrou, H.; Avgeropoulos, A.; Hadjichristidis, N.; Miller, R. D.; Thomas, E. L. *Science* **1999**, *286*, 1716−1719.
(42) Finnefrock, A. C.; Ulrich, R.; Du Chesne, A.; Honeker, C. C.; Schumacher, K.; Unger, K. K.; Gruner, S. M.; Wiesner, U. *Angew. Chem., Int. Ed.* **2001**, *40*, 1207−1211.
(43) Liu, X. Y.; Tian, B. Z.; Yu, C. Z.; Gao, F.; Xie, S. H.; Tu, B.; Che, R. C.; Peng, L. M.; Zhao, D. Y. *Angew. Chem., Int. Ed.* **2002**, *41*, 3876−3878.
(44) Flodström, K.; Alfredsson, V.; Källrot, N. *J. Am. Chem. Soc.* **2003**, *125*, 4402−4403.
(45) El-Safty, S. A.; Hanaoka, T. *Chem. Mater.* **2003**, *15*, 2892−2902.
(46) Faget, L.; Berman, A.; Regev, O. *Thin Solid Films* **2001**, *386*, 6−13.
(47) Nishiyama, N.; Park, D. H.; Koide, A.; Egashira, Y.; Ueyama, K. *J. Membr. Sci.* **2001**, *182*, 235−244.
(48) Alberius, P. C. A.; Frindell, K. L.; Hayward, R. C.; Kramer, E. J.; Stucky, G. D.; Chmelka, B. F. *Chem. Mater.* **2002**, *14*, 3284−3294.
(49) Coleman, N. R. B.; Attard, G. S. *Microporous Mesoporous Mater.* **2001**, *44*, 73−80.

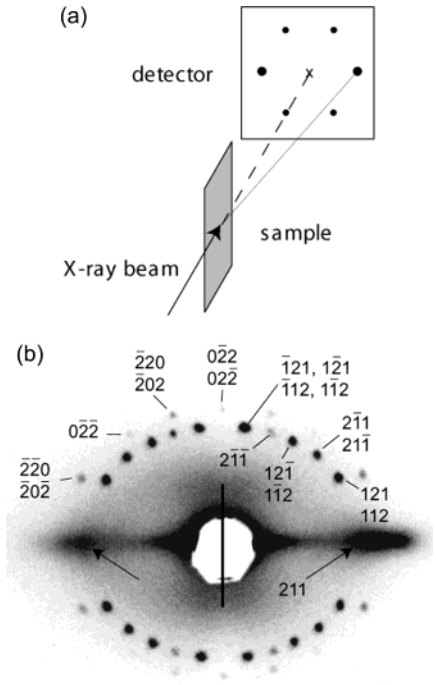

Figure 1. (a) Schematic diagram of the experimental configuration for glancing incidence small-angle X-ray scattering experiments. (b) SAXS pattern from a 600-nm-thick film of as-synthesized mesostructured $C_{16}EO_{13}$/silica with the $Ia\bar{3}d$ bicontinuous cubic structure. The X-ray beam was incident on the film at an angle of 4° from parallel. The film plane is indicated by the vertical line. For clarity, the 211 reflections along the inner ellipse are labeled only in the first quadrant, while the 220 reflections along the outer ellipse are labeled only in the second. Indices of unlabeled spots in these quadrants are found by inverting those of the corresponding spots from the opposing quadrant. Indices of spots in the lower half of the pattern are identical to those of the corresponding spots in the upper half as a result of the rotational symmetry about the direction normal to the film plane.

flight mass spectrometry was performed using a Thermo Bioanalysis Dynamo system, following the procedure of Cumme et al.[50] The batch of surfactant used in the present study was found to have a number-average molecular weight (M_n) corresponding to approximately $C_{16}EO_{13}$, with a polydispersity index (M_w/M_n) of 1.06. Hence, the surfactant will be referred to as $C_{16}EO_{13}$ in discussing the work performed here.

Two-dimensional small-angle X-ray scattering (2D SAXS) experiments were conducted on one of two instruments. The first consisted of an 18-kW Rigaku rotating Cu anode (λ = 1.54 Å) with a bent graphite monochromator and an 18-cm-diameter Mar image plate detector. The sample-to-detector distance was 713 mm, allowing investigation of length scales from ~1 to 10 nm. The second beam line consisted of a fine focus 0.2-mm Rigaku rotating Cu anode (λ = 1.54 Å) and a Bruker HI-STAR multiwire area detector, operated with a sample-to-detector distance of 1510 mm, covering scattering from real-space structures with sizes of ~5−50 nm. Patterns were recorded with the X-ray beam incident at an angle of ~2−4° from parallel to the film plane, as illustrated schematically in Figure 1a. We refer to this configuration as "glancing incidence" to distinguish it from the technique of "grazing incidence" SAXS, wherein the X-ray beam is incident at nearly the critical angle.[51]

Transmission electron microscopy (TEM) measurements were conducted on a JEOL 2000FX microscope operating at 200 kV. Plan-view samples were prepared by transferring small pieces of mesoporous silica films that had detached from the substrate during calcination onto a copper TEM grid. Cross-sectional samples were prepared by focused-ion-beam milling with an FEI DB235 system. Simulated TEM volume projections were calculated by following an approach described by Thomas, Hoffman, and co-workers.[37,52] The locations of the pore walls were simulated using the approximate equation for the triply periodic gyroid minimal surface:[53]

$$g(x,y,z) = \sin(2\pi x/a)\cos(2\pi y/a) + \sin(2\pi y/a)\cos(2\pi z/a) + \sin(2\pi z/a)\cos(2\pi x/a) \quad (1)$$

where a is the cubic lattice parameter. Setting $g(x,y,z) = \pm b$ gives rise to two enantiomorphic surfaces, each describing the boundary of an enclosed 3D network of channels, where points (x,y,z) for which $|g(x,y,z)| > b$ comprise the pore interiors.[37] A value of b = 1.13 was chosen, corresponding to a structure with 25% porosity, as this is the approximate volume fraction of the hydrophobic component of the cubic phase in the Brij-56/water system, assuming that the poly(ethylene oxide) chains are located completely in the hydrophilic regions. For each pixel of the simulated volume projections, numerical integration of the mass thickness was performed along the desired projection direction (i.e., normal to the projected image plane). The value of $g(x,y,z)$ was calculated for evenly spaced points along this direction: points found to lie within the silica wall ($|g| < b$) contributed a value of 1 to the mass thickness, whereas those in the pore channels ($|g| \geq b$) contributed 0. The values of projected mass thicknesses were linearly mapped onto gray scale images, with zero corresponding to white, and tiled to produce images with dimensions comparable to those of the experimentally obtained micrographs.

Scanning force microscopy (SFM) images were recorded using a Digital Instruments Dimension 3100 microscope operated in tapping mode. Optical micrographs were collected in reflection mode under conditions of Nomarski differential interference contrast.

Results and Discussion

Bicontinuous Cubic Mesostructured Silica Films. To characterize mesostructural ordering in the silica thin films, glancing incidence 2D SAXS was employed. Figure 1b shows a typical scattering pattern obtained from a ~600-nm-thick silica/surfactant film with a bicontinuous cubic mesostructure, synthesized with an estimated composition of 60 vol % Brij-56 at a temperature of 45 °C. A number of discrete and well-resolved diffraction spots are seen, distributed along two ellipses. These spots occur on ellipses rather than circles due to the anisotropic shrinkage of the mesostructured silica film that occurs perpendicular to the substrate as the film dries and the silica framework cross-links and densifies.[54,55] The ratio of the axes (both major and minor) of the outer ellipse to those of the inner ellipse is 1.155, which agrees very well with the predicted value of $(8/6)^{1/2} = 1.155$ for the 211 and 220 reflections, the first two allowed reflections for the $Ia\bar{3}d$ space group.[56] Furthermore, the intensities of the diffraction spots on the outer ellipse are approximately 20% of those along the inner ellipse, which agrees well with experimentally observed values of the intensities for the 211 and 220 reflections in powder X-ray diffraction patterns for similar systems.[21,30,36,43,57] No reflections were observed at larger scattering angles, also in reasonable

(50) Cumme, G. A.; Blume, E.; Bublitz, R.; Hoppe, H.; Horn, A. *J. Chromatogr. A* **1997**, *791*, 245−253.
(51) Als-Nielsen, J.; McMorrow, D. *Elements of Modern X-ray Physics*; Wiley: New York, 2001.
(52) Anderson, D. M.; Bellare, J.; Hoffman, J. T.; Hoffman, D.; Gunther, J.; Thomas, E. L. *J. Colloid Interface Sci.* **1992**, *148*, 398−414.
(53) von Schnering, H. G.; Nesper, R. *Z. Phys. B: Condens. Matter* **1991**, *83*, 407−412.
(54) Klotz, M.; Albouy, P. A.; Ayral, A.; Menager, C.; Grosso, D.; Van der Lee, A.; Cabuil, V.; Babonneau, F.; Guizard, C. *Chem. Mater.* **2000**, *12*, 1721−1728.
(55) Finnefrock, A. C.; Ulrich, R.; Toombes, G. E. S.; Gruner, S. M.; Wiesner, U. *J. Am. Chem. Soc.* **2003**, *125*, 13084−13093.
(56) *International Tables for X-ray Crystallography*; Henry, N. F. M., Lonsdale, K., Eds.; Kynock Press: Birmingham, 1974; Vol. 1.
(57) Funari, S. S.; Rapp, G. *J. Phys. Chem. B* **1997**, *101*, 732−739.

agreement with previous studies which reported that the intensities of higher-order peaks are frequently low for $Ia\bar{3}d$ structures.[21,30,36,43,57] The V_1 phases in the binary phase diagrams of water with a number of oxyethylene-alkyl ether[58−60] or oxyethylene-oleyl ether[61] surfactants have been determined to correspond to the $Ia\bar{3}d$ structure.

As indicated by the arrows in the diffraction pattern in Figure 1b, there are diffraction spots located along the inner ellipse in the direction normal to the film plane,[62] establishing that the cubic mesostructure is oriented with its (211) planes parallel to the interface. This was the orientation most frequently observed for the $Ia\bar{3}d$ structure in a previous study of films of surfactant/water mixtures for a similar surfactant ($C_{12}EO_6$).[63] The (211) planes are also epitaxially parallel to the lamellar sheets of the L_α phase and the (10) planes of the 2D hexagonal phase,[64] and mesophases confined to thin film geometries tend to orient with these planes parallel to the substrate.[65−68]

While surface energy leads to mesostructures that are highly oriented in the direction normal to the film plane, the films are transversely isotropic, meaning there is typically no preferred orientation of mesostructured grains within the plane.[24,48,54] The reciprocal space scattering intensity can then be considered as a series of circular rings that lie parallel to the plane of the film. The rings are swept out by diffraction spots as the pattern for a single-crystal-like sample is rotated through an angle of 360° about the [211] axis (normal to the film plane). The plane of the detector intersects each ring twice, yielding two spots for each (one in the top half of the scattering pattern and one in the bottom). Because each of the constituent rings may correspond to a different number of permutations of the indices *hkl*, the observed spots for a given set of crystallographically equivalent reflections are not necessarily of equal intensities. For example, in Figure 1b the spot indexed as arising from the 121 and 112 reflections is twice as intense as the spot indexed to the $2\bar{1}\bar{1}$ reflection.

The angles between the [211] axis and each of the crystallographically equivalent directions were calculated as illustrated for the [112] direction:

$$\phi = \cos^{-1}\left(\frac{[211]\cdot[112]}{|[211]||[112]|}\right) = 33.6° \qquad (2)$$

This yields a set of predicted angles relative to the [211] axis at which reflections should occur and the anticipated multiplicity for each. This procedure was then repeated for all of the 220 reflections. Finally, a stretching operation along the direction normal to the film plane was applied to the predicted diffraction pattern to account for the anisotropic shrinkage of the film that occurs as the silica dries and cross-links.[69] Using this approach, the positions of the spots in Figure 1b could all be assigned as the 211 and 220 reflections of a distorted cubic structure. Note that most spots in Figure 1b have several indices, corresponding to the degeneracy induced by the transverse isotropy of the sample. The relative intensities of the diffraction spots corresponded very well to the predicted multiplicities. While the assignments of the diffraction spots to the 211 and 220 reflections of a cubic phase do not strictly establish the space group, the data are consistent with previous scattering data for the $Ia\bar{3}d$ structure in surfactant and lipid systems,[57,70] block copolymers,[36] and mesoporous silicas[21,30,43] but inconsistent with data for the two other known bicontinuous cubic structures with space groups $Im\bar{3}m$[55,70] and $Pn\bar{3}m$.[57,70] Thus, it can be confidently concluded that the $C_{16}EO_{13}$/silica V_1 phase seen here corresponds to a distorted $Ia\bar{3}d$ (double-gyroid) structure.

The narrow width of the region over which the V_1 phase is observed in the Brij-56/water system[49] implies that the cubic phase is never far from a phase boundary with either the lamellar or the 2D hexagonal phase. Given the multicomponent and nonequilibrium process by which mesostructured silica is prepared, it was anticipated that the proximity of these phase boundaries might give rise to heterogeneous mesostructural ordering of the $C_{16}EO_{13}$/silica films. The ability to identify and understand these heterogeneities is crucial if the mesostructured films are to be used in applications where the mesoscale architecture must be precisely controlled. For films prepared with an estimated 59−60 vol % $C_{16}EO_{13}$ and aged at 45 °C, scattering patterns similar to the one shown in Figure 1b were typically observed. In most cases, however, diffraction spots were observed along the direction normal to the film plane at slightly smaller scattering vector q than that of the 211 spots of the cubic phase, indicating the presence of a mixed-phase structure. The extra spots correspond to the first-order reflections from a lamellar structure, with lamellar sheets oriented parallel to the film plane.

TEM was used to investigate the mixed-phase structure of the silica films, as well as to support the assignment of the $Ia\bar{3}d$ structure. Low-magnification images taken with the electron beam directed perpendicular to the film plane, such as in Figure 2a, reveal contrast between regions with different mesostructural ordering that have well-demarcated interfaces between them. The lighter central region shows no apparent mesoscale features, consistent with the SAXS results indicating a lamellar structure with sheets oriented parallel to the plane of the film. The darker regions around the periphery of the lamellar region correspond to domains of the cubic structure observed in the X-ray measurements, as established by the high-magnification plan-view image shown in Figure 2b. A series of striped features are observed running parallel to the long edge of the cubic domain that closely resemble the features in a simulated volume projection along the [211] zone axis of a double-gyroid structure shown in Figure 2c. The stripes in the simulated image correspond to the $(0\bar{1}1)$ planes; the

(58) Clerc, M.; Levelut, A. M.; Sadoc, J. F. *J. Phys.* **1990**, *51*, C797−C7104.
(59) Funari, S. S.; Rapp, G. *Proc. Natl. Acad. Sci. U.S.A.* **1999**, *96*, 7756−7759.
(60) Impéror-Clerc, M.; Levelut, A. M. *Eur. Phys. J. E* **2001**, *4*, 209−215.
(61) Kunieda, H.; Shigeta, K.; Ozawa, K.; Suzuki, M. *J. Phys. Chem. B* **1997**, *101*, 7952−7957.
(62) The intensities of the 211 reflections normal to the film plane (see arrows) observed in Figure 1b are relatively weak, since the incident X-ray beam was several degrees away from the Bragg condition for (211) planes oriented parallel to the film surface.
(63) Pieranski, P.; Sittler, L.; Sotta, P.; Impéror-Clerc, M. *Eur. Phys. J. E* **2001**, *5*, 317−328.
(64) Rançon, Y.; Charvolin, J. *J. Phys. Chem.* **1988**, *92*, 2646−2651.
(65) Krausch, G. *Mater. Sci. Eng. R−Rep.* **1995**, *14*, 1−94.
(66) Coulon, G.; Russell, T. P.; Deline, V. R.; Green, P. F. *Macromolecules* **1989**, *22*, 2581−2589.
(67) Anastasiadis, S. H.; Russell, T. P.; Satija, S. K.; Majkrzak, C. F. *Phys. Rev. Lett.* **1989**, *62*, 1852−1855.
(68) Henkee, C. S.; Thomas, E. L.; Fetters, L. J. *J. Mater. Sci.* **1988**, *23*, 1685−1694.
(69) A linear distortion in real space along a crystallographic axis of a cubic structure produces a reciprocal linear distortion of the diffraction pattern along the corresponding reciprocal space direction. The stretching required to match the predicted and experimental diffraction patterns varied from 15 to 20% depending on the exact synthesis conditions. For the pattern in Figure 1b, the stretching required was 20%.
(70) Mariani, P.; Luzzati, V.; Delacroix, H. *J. Mol. Biol.* **1988**, *204*, 165−188.

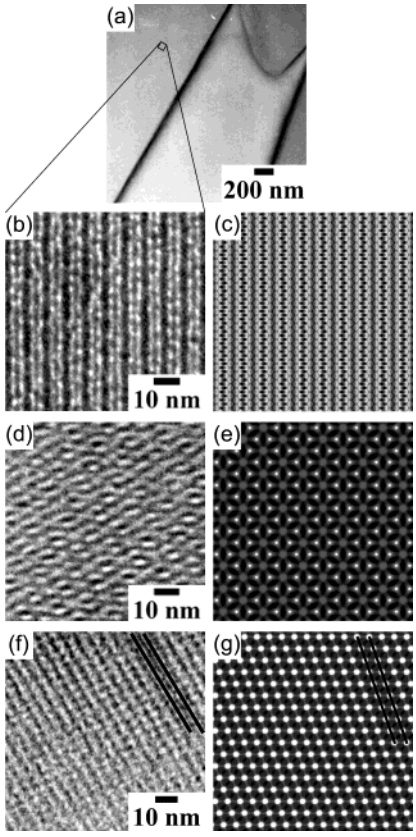

Figure 2. Experimental and simulated TEM images for $Ia\bar{3}d$ cubic mesostructured silica films. (a) Low-magnification plan-view image showing contrast between a lamellar mesostructure in the central area and cubic domains at the edges. (b) High-magnification plan-view image (along the [211] zone axis) taken in a location indicated approximately by the box drawn in the low-magnification image and (c) simulated [211] volume projection. (d) Cross-sectional image taken with the electron beam along the $[\bar{1}11]$ zone axis and (f) simulated $[\bar{1}11]$ volume projection. (g) Cross-sectional image along the $[01\bar{1}]$ zone axis and (h) simulated $[01\bar{1}]$ volume projection. All samples were calcined, except that in image f, which was as-synthesized.

orientation of the corresponding stripes in the micrograph indicates that the long edges of the cubic domains correspond to the $(0\bar{1}1)$ and $(01\bar{1})$ facets. The d_{110} spacing is estimated from the micrograph to be 9.1 nm, corresponding to a cubic lattice parameter of $|a| = 13$ nm. This is in agreement with the SAXS experiments that yield an intersection of the 211 ellipse with the film plane at $d = 5.6$ nm, corresponding to a lattice parameter of $|a| = 14$ nm.

To provide views of the cubic mesostructure along other crystallographic directions, cross-sectional TEM samples were prepared by focused ion beam milling. Thin (~150-nm) slices were taken perpendicular to the long and short axes of the cubic grains, which provided views of the structure along the $[\bar{1}11]$ and the $[01\bar{1}]$ zone axes, respectively. The micrograph taken with the electron beam along the $[\bar{1}11]$ direction in Figure 2d shows contrast similar to the "wagon-wheel" pattern typically observed for the [111] direction of the double-gyroid structure,[34,36] as does the simulated volume projection shown in Figure 2e. Note that the simulated image has been computed for a true $Ia\bar{3}d$ cubic structure; comparison to the cross-sectional TEM image in Figure 2d reveals the compression of the structure that has occurred normal to the substrate, due to anisotropic shrinkage of the film. The electron micrograph in Figure 2f was taken along the $[01\bar{1}]$ axis of a cubic domain, and the contrast is similar to the calculated projection along this axis in Figure 2g. Once again, the distortion of the structure is evident by comparison of the two images. Lines have been drawn to indicate the dominant feature of the experimental micrograph and what appear to be the corresponding planes of the simulated image. The mismatch in angle between the two is presumed to arise predominantly from compression of the structure as the film shrinks. The TEM data taken together strongly support the $Ia\bar{3}d$ double-gyroid structural assignment, its orientation with the (211) planes parallel to the film plane, and the correspondence of the long edges of the rectangular grains to the $(0\bar{1}1)$ and $(01\bar{1})$ facets. The absence of any mesostructural features in the surrounding regions of the film corroborates the SAXS data, indicating that these areas correspond to a lamellar structure.

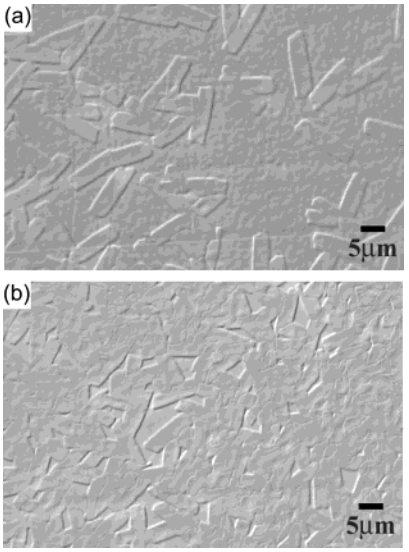

Figure 3. Optical micrographs of 600-nm-thick as-synthesized mixed-phase mesostructured $C_{16}EO_{13}$/silica films showing $Ia\bar{3}d$ cubic domains, interspersed by lamellar regions. (a) Isolated cubic domains display clear faceting. (b) As the surface coverage of the cubic phase increases, the domains impinge upon each other, making the faceting less obvious.

Mixed-Phase Film Structures. Macroscopic texturing of the mesoscopically ordered silica/$C_{16}EO_{13}$ films with mixed-phase structures was examined in detail using optical microscopy and SFM. Figure 3 contains optical micrographs of an as-synthesized mesostructured silica thin film that was determined from SAXS measurements to correspond to a mixture of $Ia\bar{3}d$ cubic and lamellar structures. The faceted rectangular features evident in Figure 3a, which were also observed by TEM [Figure 2a], correspond to single-crystal-like domains of the $Ia\bar{3}d$ cubic structure. The elongated shapes of these domains resemble closely what has been observed by Impéror-Clerc and coworkers[63] for the $Ia\bar{3}d$ phase in the binary $C_{12}EO_6$/water system when cubic domains are grown slowly in a film geometry with (211) planes parallel to the substrate. The long edges of the rectangular regions seen in the micrographs presented here correspond to the $(01\bar{1})$ and $(0\bar{1}1)$ facets of the cubic structure,[63] in agreement with the TEM results of Figure 2. The shorter edges do not appear to be clearly faceted, which is also consistent with observations made for the binary $C_{12}EO_6$/water system, where these edges did not develop clear faceting until domain growth was complete.[63] In Figure 3b, the $Ia\bar{3}d$ cubic grains cover the majority of the substrate surface and impinge on one another, partially obscuring their rectangular shapes.

In nearly all cases where the bicontinuous cubic structure was observed, the $C_{16}EO_{13}$/silica films were

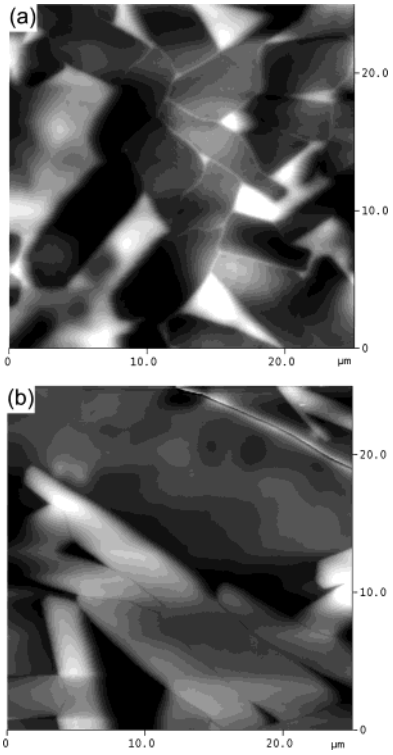

Figure 4. Scanning force microscope height-contrast images of a mixed-phase mesostructured silica film with $Ia\bar{3}d$ cubic domains visible, where bright areas are higher than dark areas. (a) As-synthesized silica/Brij-56 film of thickness 600−700 nm, with a total height scale (from black to white) of 130 nm. (b) A section of the same sample following calcination, where the film thickness is reduced to 300−400 nm. The total height scale is 220 nm.

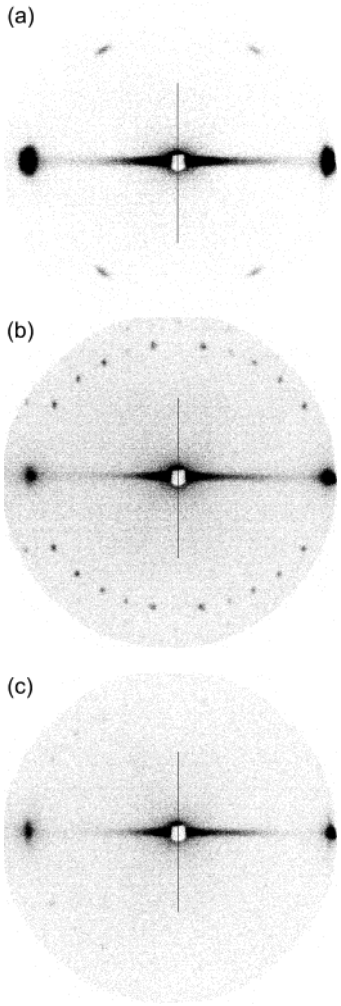

Figure 5. Glancing incidence SAXS patterns collected from three mesostructured silica films made with the same composition (60 vol % Brij-56) and aged at temperatures of (a) 37 °C, (b) 45 °C, and (c) 47 °C.

characterized by the presence of mixed phases. The surface coverage by the $Ia\bar{3}d$ cubic structure ranged anywhere from a few scattered grains to approximately 95% of the film surface, depending on the conditions of film synthesis and processing. The mixed-phase structure may reflect a region of pseudo-equilibrium two-phase coexistence in the quasi-lyotropic-liquid-crystalline state of the hydrated silica/surfactant film formed after dip-coating. Equilibrium two-phase coexistence regions are expected for first-order phase transitions in lyotropic liquid crystals[71] and have been identified at the boundaries of the V_1 phase in several poly(oxyethylene)-alkyl ether surfactant/water systems.[63,72−75] An alternative explanation for the mixed-phase structure is that cross-linking of the silica network quenches the system before the entire film has had time to adopt the cubic structure, consistent with a previous observation of silica polymerization leading to kinetic trapping of spatially heterogeneous silica mesostructures.[76] Both the lamellar and 2D hexagonal phases have been found to be metastable relative to the bicontinuous cubic phase in the $C_{12}EO_6$/water system, and cubic domains were found to grow slowly under conditions of low supersaturation.[63] The ubiquity of the mixed-phase structures seen here suggests that kinetic effects are important in determining the structures of $C_{16}EO_{13}$/silica films; however, it is difficult to establish this point conclusively due to the inherently nonequilibrium nature of the system. It is quite possible that both kinetic-trapping and phase-coexistence effects play a role in determining the mixed-phase film structure. While the films studied here typically consisted of a mixture of cubic and lamellar structures, careful control of the synthesis conditions allows for the preparation of films with predominantly (∼95%) cubic structure.

SFM height images (Figure 4) of mesostructured $C_{16}EO_{13}$/silica and mesoporous silica films show that the cubic domains have different thicknesses than the surrounding lamellar structures. Typically, the grains of cubic structure were 80−110 nm thinner than surrounding regions in as-synthesized films (film thickness, 600−700 nm) and 60−100 nm thicker in films where the surfactant template had been removed by calcination (thickness, 300−400 nm). The reversal in the relative heights of the cubic domains and the surrounding areas upon calcination further corroborates that the surrounding areas correspond to a lamellar mesophase. Upon removal of the surfactant species, lamellar silica mesostructures typically collapse, leading to a large decrease in local film thickness. The reason for the initial difference in thickness between the cubic domains and surrounding areas is not completely

(71) Holmes, M. C.; Leaver, M. S. In *Phase Transitions in Complex Fluids*; Tolédano, P., Figueiredo Neto, A. M., Eds.; World Scientific: Singapore, 1998; pp 29−55.
(72) Fairhurst, C. E.; Holmes, M. C.; Leaver, M. S. *Langmuir* **1997**, *13*, 4964−4975.
(73) Inoue, T.; Matsuda, M.; Nibu, Y.; Misono, Y.; Suzuki, M. *Langmuir* **2001**, *17*, 1833−1840.
(74) Zheng, L. Q.; Suzuki, M.; Inoue, T.; Lindman, B. *Langmuir* **2002**, *18*, 9204−9210.
(75) Zheng, L. Q.; Suzuki, M.; Inoue, T. *Langmuir* **2002**, *18*, 1991−1998.
(76) Melosh, N. A.; Davidson, P.; Chmelka, B. F. *J. Am. Chem. Soc.* **2000**, *122*, 823−829.

understood and remains under investigation; however, it is consistent with the observation from SAXS that the spacing between (211) planes of the cubic structure is smaller than that between the epitaxially parallel lamellar sheets.

Dependence of Silica Mesostructure on Aging Temperature. Formation of the bicontinuous cubic structure was found to be highly sensitive to the conditions of $C_{16}EO_{13}$/silica film preparation. Changing the aging temperature by a few degrees Celsius caused the system to adopt 2D hexagonal or lamellar architectures, instead of the $Ia\bar{3}d$ cubic structure. To study the dependence of mesostructural ordering on temperature, thin films were prepared with an estimated 60 vol % surfactant from a single precursor solution and subsequently aged at different temperatures. SAXS patterns obtained from three such films prepared over the temperature range 37−47 °C are shown in Figure 5. At an aging temperature of 37 °C, a (distorted) 6-fold symmetric pattern was observed, which is indicative of 2D hexagonal ($P6mm$) mesostructural ordering.[54] At 45 °C, the characteristic reflections of the $Ia\bar{3}d$ structure were observed, and no strong lamellar reflections were present, indicating the presence of a nearly single-phase bicontinuous cubic mesostructure. Some faint intensity spots from the cubic phase could still be observed at an aging temperature of 47 °C. However, the dominant features of the scattering in this case were strong reflections normal to the film plane, consistent with a primarily lamellar mesostructure. Optical microscopy confirmed that this film had a mixed-phase structure with a small number of isolated cubic domains present. Comparison of these data to the Brij-56/water $T-x$ phase diagram[49] shows that both systems have the same progression of phases (2D hexagonal → bicontinuous cubic → lamellar) with increasing temperature in this region of composition.[77,78]

Conclusions

The synthesis and characterization of mesoscopically ordered $C_{16}EO_{13}$/silica thin films with bicontinuous cubic structure (space group $Ia\bar{3}d$) have been described. The procedure for preparing such films, while highly sensitive to composition and temperature, is straightforward and was derived by direct comparison to the established phase behavior of the structure-directing surfactant species in binary mixtures with water. Small-angle X-ray scattering and TEM establish that the cubic phase has the $Ia\bar{3}d$ double-gyroid structure and is oriented with its (211) crystallographic planes parallel to the substrate. The films are comprised of faceted cubic domains that typically coexist with a lamellar phase. In the narrow region of synthesis space investigated (59−60 vol % $C_{16}EO_{13}$; 37−47 °C), the "phase" behavior of the surfactant/silica system is similar to that in binary Brij-56/water mixtures, with the same progression of architectures (2D hexagonal → bicontinuous cubic → lamellar) occurring as temperature is increased. The ability to influence the mesostructural ordering of these films by small adjustments in temperature is a potentially important variable for influencing macroscopic film properties. In particular, controlling the structural uniformity of mesoporous silica films with bicontinuous cubic structures will be important for their eventual applications in membrane separations, as sensors, or as hosts for nanoscale materials syntheses.

Acknowledgment. We thank Dr. Patrick Davidson and Professor Galen Stucky for helpful discussions, Mario Yasa and Heather Evans for help with the SAXS measurements, and Jan Löfvander for assistance with the preparation of cross-sectional TEM samples. R.H. gratefully acknowledges support from the U.S. National Science Foundation for a Graduate Research Fellowship and the Corning Foundation for a Fellowship in Materials Research. This work was supported by the U.S. National Science Foundation through Award DMR-02-33728, through the MRSEC program under Award DMR-00-80034, and with travel support from the Division of International Programs under Grant INT-9726744.

LA030442Z

(77) The appearance of the cubic phase at ~45 °C in the $C_{16}E_{13}$/silica system (at ~60 vol % surfactant) occurs at a somewhat lower volume fraction than in the binary Brij-56/water system (~70 vol % surfactant). This suggests that the simple approach followed here may underestimate slightly the surfactant volume fraction in the as-synthesized dip-coated film. This is likely due to the influence of the temperature at which the film is processed on the film composition. The hydrophilic content (and hence the mesostructure) of surfactant/silica films has been shown to depend on the relative humidity of the surroundings (see ref 78). As the temperature of the system is raised above room temperature, the films desorb water, thereby increasing the relative surfactant content. This favors formation of the cubic phase at lower initial surfactant content than expected, based on a consideration of the surfactant−water $T-x$ phase diagram.

(78) Cagnol, F.; Grosso, D.; Soler-Illia, G.; Crepaldi, E. L.; Babonneau, F.; Amenitsch, H.; Sanchez, C. *J. Mater. Chem.* **2003**, *13*, 61−66.